Anisotropy and Lorentz-force dependence of twin-boundary pinning and its effect on flux-lattice melting in single-crystal $YBa_2Cu_3O_{7-\delta}$

Steven Fleshler,* Wai-Kwong Kwok, Ulrich Welp, Valerii M. Vinokur, Morag K. Smith, John Downey, and George W. Crabtree

Materials Science Division, Argonne National Laboratory, Argonne, Illinois 60439

(Received 13 November 1992)

The magnetoresistance of both twinned and detwinned single crystals of $YBa_2Cu_3O_{7-\delta}$ was measured as a function of magnetic field strength, orientation, and temperature to determine the pinning properties of twin boundaries and their effect on the flux-lattice melting transition. Pinning by twin boundaries manifests itself as a drop in the resistance for magnetic fields oriented within a "depinning angle" of the twin boundaries. The onset of twin-boundary pinning is found to occur at the shoulder observed in the low-temperature end of the magnetic-field-broadened resistive transition for $\mathbf{H}\|c$. Two unique current to twin-boundary configurations were employed to induce vortex motion parallel or perpendicular to the twin boundaries when the magnetic field is parallel to the c axis. We find the drop in the angular-dependent resistance, the depinning angle, and the zero-resistance temperature to be enhanced when the vortices move normal to the twin boundaries indicating that the pinning barriers for this direction of flux motion are significantly larger. The depinning angle for rotations off the c axis decreases with increasing magnetic field and decreasing temperature whereas for rotations in the ab plane it is nearly field independent. For applied magnetic fields less than 4 T the depinning angle for $\mathbf{H}$ rotated off c is larger than that for $\mathbf{H}\|ab$. Strong pinning by twin boundaries competes with the flux-lattice melting transition for tilt angles less than the depinning angle, totally suppressing the transition for $\mathbf{H}\|c$. For small misalignments off the twin boundaries a second kink is observed which marks the onset of non-Ohmic behavior and which we interpret as the flux-lattice melting transition. For angles larger than the depinning angle the field-broadenend resistive transition and the flux-lattice melting transition of twinned and detwinned crystals are shown to be essentially identical.

I. INTRODUCTION

The characteristic features of the high-temperature superconductors such as the magnetic-field-broadened resistive transition have made pinning a central issue in their study. The presence of a downturn, frequently referred to as a shoulder or kink, at the foot of the resistive transition in high-quality single crystals of $YBa_2Cu_3O_{7-\delta}$ for $\mathbf{H}\|c$ (and perpendicular to the applied current J) (Refs. 1–3) implies that the phase diagram may be quite complicated. In twinned crystals for $\mathbf{H}\|c$, the shoulder is thought to separate the resistive transition into two vortex liquid regimes with linear current-voltage characteristics: (1) a high-temperature vortex liquid phase in which pinning is relatively ineffective and (2) a low-temperature vortex liquid phase in which pinning becomes effective in restricting flux motion substantially. It has been suggested that the low-temperature liquid phase is due to either the predominance of the pinning energies over thermal energies[4] or a true phase transition into a hexatic phase with enhanced viscosity.[5,6] In addition, a non-Ohmic regime has been distinguished at temperatures near the zero-resistance point of thin films[7] and twinned single crystals[3,8] and identified with the "solidification" of the vortex glass phase.[9] More recently, the existence of a sharp kink in the resistive transition of untwinned single crystals was observed to exhibit hysteretic behavior associated with flux-lattice melting.[10] However, this melting kink is not observed in all detwinned crystals presumably because of varying degrees of disorder, and "clean" and "dirty" behavior in these crystals can be distinguished by the presence or absence of the melting kink. Thus both the low-temperature liquid and solid-glass states are greatly affected by the extent of disorder in the system studied. Proton and Au-ion irradiation damage have been induced in twinned single crystals to facilitate investigation of the effects of varying disorder on the solid-glass phase.[11] The presence of a melting transition for $\mathbf{H}\|c$ in untwinned crystals in contrast to its absence in twinned crystals indicates that twin boundaries (TB's) play a major role in determining the vortex structure and its dynamics for this magnetic-field orientation. Presently, we focus on the angular dependence and anisotropy of TB pinning and its consequences on the resistive and melting transitions.[12]

Studies involving pinning by TB's take advantage of several useful features: (1) The twin planes are naturally occurring in the system, and fully oxygenated crystals can be used without introducing additional defects; (2) crystals can be cleaved to obtain sections with no or few TB's, or alternatively, the TB's can be removed without changes to the stoichiometry;[13] (3) the proposed pinning sites are readily observable optically; (4) the microstructure is stable (some irradiation-induced defects have been shown to anneal[14]); and (5) since TB's are extended planar objects, their contribution to pinning can be discerned by

angular-dependent measurements. A drawback to studying the role of TB's as pinning centers is the difficulty in controlling their density, and although one can find various crystals with very different macroscopic twin densities, the local density within a given crystal is generally nonuniform.

The planar nature of the TB's allows for the study of the interaction between vortices and two-dimensional defects. Anisotropic pinning behavior for flux motion parallel and perpendicular to the TB's might be expected. For homogeneous twin planes, pinning against motion parallel to the boundary is not expected. However, it has been clearly demonstrated by angular-dependent magnetoresistance measurements that pinning by TB's occurs when the Lorentz force is directed parallel to them.[15,16] This was explained qualitatively in terms of the location of atomic-size defects and disorder within the TB's.[15] Recent real-time imaging of flux profiles in lightly twinned single crystals with the aid of magneto-optical films revealed that at low temperature and low magnetic fields the TB's act as barriers to flux motion normal to their plane.[17] Magnetization-hysteresis measurements prior to and subsequent to detwinning single crystals have demonstrated that TB's enhance the magnetization critical currents in $YBa_2Cu_3O_{y-\delta}$.[18,19] However, for such measurements it is difficult to extract information on the dependence of pinning by TB's on the direction of the driving force, since the magnetization currents flow in closed paths and the resulting Lorentz force rotates with it about the magnetic field. Transport measurements of the critical-current density (J_c) of epitaxial films in a magnetic field with various orientations of the current with respect to the TB's indicate no dependence of J_c on the direction of the Lorentz force for $\mathbf{H}\|c$.[20] The films used in Ref. 20 contained TB's along both the $\langle 110 \rangle$ and $\langle 1\bar{1}0 \rangle$ directions, and thus the Lorentz force was directed at two angles relative to the TB's simultaneously. Transport measurements on crystals possessing one TB variant provide the possibility of orienting the Lorentz force along a single direction relative to the TB's. In the present paper, we investigate resistively the dependence of TB pinning on the direction of the Lorentz force in such crystals, using two unique contact configurations in which the current was driven in the *ab* plane either parallel or perpendicular to the TB's and a standard 45° current geometry. With these three geometries, the Lorentz force can be oriented at 0°, 45°, and 90° to the TB's for $\mathbf{H}\|c$.

Twin-boundary pinning effects have been studied extensively by various methods including angular-dependent magnetoresistance,[15,16,21] magnetization hysteresis,[18,19] field dependence of the magnetization near H_{c1},[22–24] magnetization relaxation and Meissner fraction,[24] torque measurements,[25–27] and decoration and imaging techniques.[17,28–30] Motivated by the results of some of these measurements, Blatter, Rhyner, and Vinokur[31] have proposed that TB pinning can occur only for magnetic fields oriented within some critical angle of the TB's. In the single-vortex-pinning picture, this critical angle is determined by the tilt modulus and the pinning energy associated with the suppression of the order parameter in the TB's. We extend our earlier results of TB pinning for field rotations in the *ab* plane[15] to higher magnetic fields and include measurements of TB pinning for field rotations off the *c* axis. We define a depinning angle (θ_p) as the maximum angle over which the pinning features in the angular-dependent magnetoresistance are observed and discuss our results qualitatively in terms of the concepts introduced in the critical-angle model.

The remainder of the text is organized as follows: We begin by describing the experimental setup and procedure for measuring the angular dependence of the magnetoresistance with our crossed magnetic-field technique. We divide Sec. III into five parts. In Sec. III A we present the field-broadened resistive transition with $\mathbf{H}\|c$ for several crystals with different Lorentz-force orientations relative to the TB's and show that the downturn to zero resistivity at the shoulder varies with the Lorentz-force direction. We take this result to indicate that the TB-pinning barriers depend on the relative direction of the Lorentz force. An investigation of the temperature dependence of TB pinning reveals that its onset coincides with the shoulder in the resistive transition. In Sec. III B we compare TB pinning and the associated depinning angle (θ_p) for crystals configured with different directions of the Lorentz force relative to the TB's for $\mathbf{H}\|c$. We find that the TB's reduce the resistance more significantly and pin over a much larger angular range (i.e., θ_p is larger) when the Lorentz force is oriented normal to them, supporting the idea that the TB-pinning barriers are largest for this flux-motion direction. We demonstrate that the features in our data that we associate with pinning by TB's are indeed due to the TB's, and as a consistency check, we compare similar measurements on a detwinned crystal. In Sec. III C the anisotropy of TB pinning with respect to the crystallographic axes is presented. The dynamics of vortices in the presence of TB's for the various Lorentz-force configurations is discussed with reference to various theoretical models in Sec. III D. Finally, in Sec. III E we show the development of an additional feature in the resistive transition as the magnetic field is tilted off the *c* axis. For large misalignments with the *c* axis, we associate this kink with the flux-lattice melting transition and show that it is strongly affected by TB pinning when the misalignment is less than the depinning angle.

II. EXPERIMENT

Twinned single crystals of $YBa_2Cu_3O_{7-\delta}$ were grown using a self-flux method described elsewhere.[32] The crystals were oxygenated at 420 °C for several days producing samples with transition temperatures in excess of 90 K and transition widths of $\Delta T_c \leq 0.5$ K, as determined from the zero-field resistive transition. We shall define T_c by the peak in the temperature derivative of the zero-field resistive transition. Crystals containing both $\langle 110 \rangle$ and $\langle 1\bar{1}0 \rangle$ twin boundaries were cleaved with a razor blade to obtain rectangular prisms containing only one twin orientation. The cleave planes were chosen to obtain the appropriate geometry for application of the measuring current in the *ab* plane with three distinct orientations

relative to the TB's: 0° (parallel), 45°, and 90° (perpendicular). These crystals shall henceforth be referred to as Y0, Y45, and Y90, respectively, and their current configuration is shown in Fig. 1. Typical TB spacings in the crystals used in this experiment were approximately 1000–2000 Å, but could vary by a factor of 4 or 5 in some crystals as determined by transmission electron and optical microscopies. In addition, two crystals referred to as DT1 and DT2 were detwinned by annealing in flowing oxygen under uniaxial stress.[13] The resulting samples were platelets with typical dimensions of the *ab* planar face being 0.7 mm × 0.3 mm and the thickness along the *c* axis varying from 0.05 to 0.15 mm.

dc and low-frequency (17-Hz) ac resistivities were measured using a standard four-probe technique with current densities on the order of 1 A/cm^2 applied in the *ab* plane. Contact pads were placed on the crystal with silver epoxy and sintered at 420 °C in flowing oxygen. Subsequently, gold wires were attached to these contact strips with silver epoxy and cured at 120 °C. Contact resistances less than 1 Ω were obtained with this method.

The three distinct current-to-TB geometries measured are represented in Fig. 1. For the two crystals Y0a and Y0b, the current was driven nominally parallel to the TB's to induce vortex motion perpendicular to the TB's when $\mathbf{H}\|c$. Y90 was configured with the current normal to the twin planes, the appropriate current arrangement to study the crystallographic anisotropy of TB pinning since for both orientations $\mathbf{H}\|ab\|$TB and $\mathbf{H}\|c\|$TB the maximum Lorentz force is realized ($H\perp J$).[21] The resulting Lorentz force for both magnetic-field orientations in this geometry was parallel to the TB's. Y45 had the conventional orientation in which the transport current was driven at 45° to the TB's. For clarity, the crystals will also be labeled with the direction of the Lorentz force relative to the TB's for $\mathbf{H}\|c\|$TB when convenient. A comparison of the results for the three different current orientations with respect to the TB's and the magnetic-field orientation $\mathbf{H}\|c\|$TB allows for the investigation of the anisotropic pinning properties of the TB's.

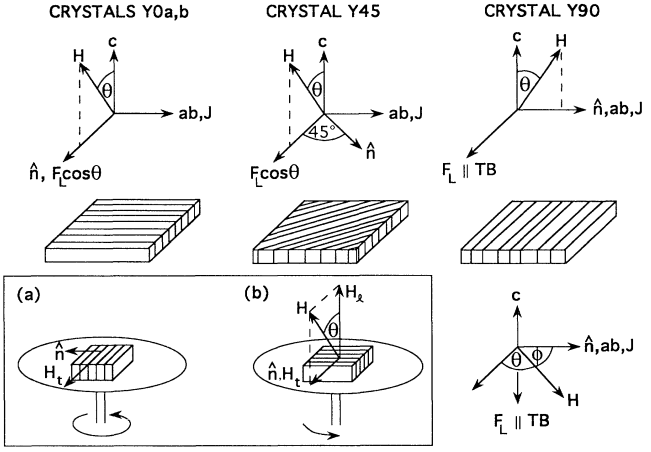

FIG. 1. Three different current-to-twin-boundary geometries and the corresponding component of the Lorentz force (F_L) in the *ab* plane. $\mathbf{H}_t$ and $\mathbf{H}_l$ denote the transverse and longitudinal magnetic fields, respectively, and $\hat{\mathbf{n}}$ is the TB normal. For crystal Y90 we also show the magnetic field rotated in the *ab* plane, and for this case the angles θ and $\phi = 90° - \theta$ describe the field orientation relative to the TB's and current, respectively. The inset shows the procedure for orienting the crystals Y90 and Y0 for the crossed-field technique.

The angular dependence of the resistivity was measured by placing the crystals in the bore of two orthogonal superconducting magnets, an 8-T longitudinal magnet and a 1.5-T transverse split coil. The resultant magnetic field was tilted relative to the sample by fixing the two orthogonal compounds of the magnetic field independently. This "crossed-field" technique yields an extremely high angular resolution of 0.005°.[33] However, we were limited at high fields in our maximum attainable angle because of the constraint imposed by the size of the transverse magnetic field. To provide additional rotational freedom, the sample was mounted on a stage which could be mechanically rotated about the longitudinal magnetic field (see the inset of Fig. 1). We have previously employed such a method to demonstrate intrinsic pinning by the layered crystal structure of $YBa_2Cu_3O_{7-\delta}$.[33]

In order to achieve a precise orientation of the sample, we use the sharp drops observed in the angular dependence of the resistance for $\mathbf{H}\|$TB as a reference. Figure 2 shows $R(\theta)$ at a fixed temperature for the mechanical ro-

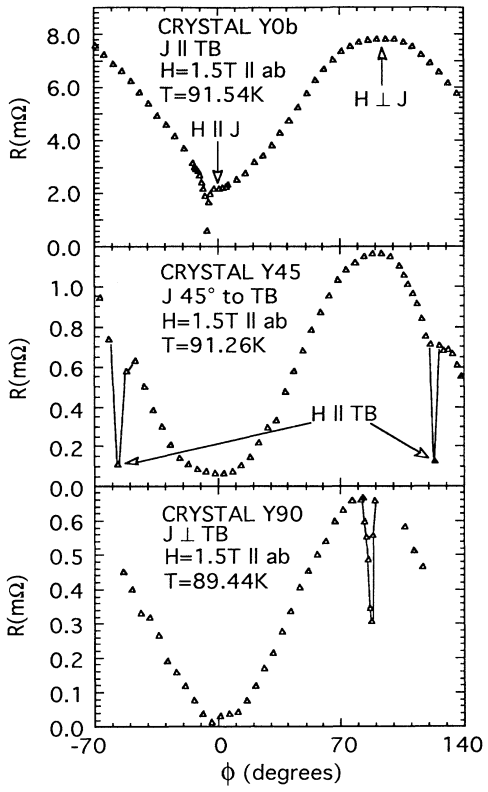

FIG. 2. Angular dependence of the resistance for the three distinct current configurations at fixed temperature for a magnetic field of 1.5 T rotated in the *ab* plane. Sharp drops in the resistance when the magnetic field is nearly aligned with the TB's are superimposed on the flux-flow $\sin^2\phi$ behavior.

tation of three of these crystals in a 1.5-T magnetic field confined to the *ab* plane with ϕ measured relative to the current direction. Sharp drops in the resistance due to TB pinning[15,16] are superimposed on the smooth $\sin^2\phi$ flux-flow behavior[15] when the magnetic field is nearly aligned with the TB's. Note that for crystal Y0b the TB-pinning dip is observed when the magnetic field was oriented approximately 6° off the current direction. This indicates the misalignment of the current with respect to the TB's. For crystal Y0a we find the misalignment to be approximately 3° in the same manner. As demonstrated by the angular scan for Y90 ($J\perp$TB), the drops in the resistance are sharp enough to mechanically align the magnetic field parallel to the TB's within 0.5°. To facilitate probing the angular region about the TB's, we employ the crossed-magnetic-field technique mentioned earlier. Our procedure for measuring TB pinning with this method is as follows: (1) The crystal is mounted with the longitudinal magnetic field ($\mathbf{H}_l$) nominally parallel to the TB's either $\mathbf{H}_l \| c \|$TB or $\mathbf{H}_l \| ab \|$TB. (2) The crystal is mechanically rotated in the transverse magnetic field ($\mathbf{H}_t$) while monitoring the resistance, and $\mathbf{H}\|$TB is located by the minimum in the TB-pinning dip [see Fig. 1(a), inset]. (3) The crystal is then manually rotated so that the transverse magnetic field is in the desired plane of rotation either 0°, 45°, or 90° to the TB's [see Fig. 1(b), inset]. (4) The net magnetic field is then rotated in the chosen plane of rotation by applying both $\mathbf{H}_l$ and $\mathbf{H}_t$ simultaneously while maintaining a constant resultant magnitude [see Fig. 1(b), inset].

For measurement of the depinning angle θ_p for rotations off the *c* axis, we have chosen to rotate the magnetic field in the plane containing the *c* axis and the TB normal for crystals Y0a, Y0b, and Y90 (see Fig. 1). For crystal Y90 the current is contained in the plane of rotation, and although the direction of the Lorentz force is not altered upon rotation, its magnitude decreases as $\cos\theta$. For crystals Y0a and Y0b ($J\|$TB), the plane of rotation is perpendicular to the current, and consequently, the magnitude of the Lorentz force is unaffected by the rotation. However, the direction of the Lorentz force changes, and as the field is rotated off the *c* axis by an angle θ, the Lorentz force rotates off the *ab* plane by the same amount. We note that the component of the Lorentz force in the *ab* plane (and normal to the TB) decreases as $\cos\theta$ as the magnetic field is rotated off the *c* axis. For the angular range over which TB's pin ($\theta_p \sim 20°$) for crystals Y0a and Y0b, the component along the TB (proportional to $\sin\theta$) is much smaller than the normal component and the situation is approximately the same as that for Y90. For the crystal configured with the current oriented 45° to the TB's, we rotate the field off the *c* axis in the plane normal to the current. For such a case, the Lorentz force has a component in the *ab* plane proportional to $\cos\theta$ directed at 45° to the TB's and a component along the *c* axis parallel to the TB's which varies like $\sin\theta$. We can apply the same arguments for this geometry as for that of Y90. We shall not present angular scans of the magnetoresistance for the 45° configuration here. For analogous data on a crystal with both types of twin domains and the magnetic field rotated in the plane bisecting the TB's (i.e., for the same type of Lorentz-force configuration), we refer the reader to Ref. 34. Note that for $\theta = 0°$ ($\mathbf{H}\|c$) the Lorentz force is in the *ab* plane for all three current configurations.

III. RESULTS

The resistivity normalized relative to its value at T_c versus reduced temperature T/T_c with $\mathbf{H} = 4$ T $\|c$ is plotted for crystals with various directions of the Lorentz force relative to the TB's in Fig. 3. The data are presented in this manner to compensate for small variations in T_c and the normal-state resistivity. The resistive transitions appear remarkably similar at high reduced temperatures, but deviate significantly below the shoulder at $T/T_c \approx 0.93$ as indicated by the solid arrow. The transitions of crystals Y0a and Y0b ($F_L \perp$TB) exhibit the sharpest downturn toward zero resistivity. As the angle between the Lorentz force and the TB's is decreased, the downturn at $T/T_c \approx 0.93$ becomes less pronounced and the zero-resistance point progresses to lower reduced temperatures. The shoulder for crystal Y90 ($F_L \|$TB) is practically smeared out and the field-broadened transition is reminiscent of those observed for "dirty" detwinned single crystals (as will be discussed in Sec. III B). These data suggest that the downturn marks the onset of TB pinning and that the pinning strength increases monotonically with the angle between the driving force and the TB's. We probed all of these crystals using our crossed-field technique for TB pinning in the temperature regime below the resistive downturn with this hypothesis in mind.

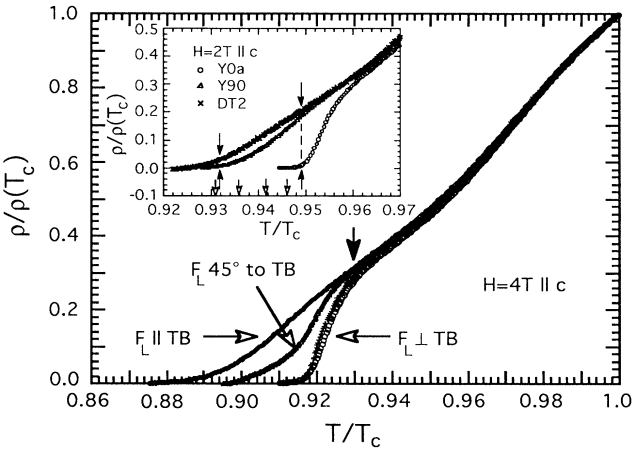

FIG. 3. Resistivity normalized to its value at T_c vs reduced temperature for four crystals with three different current-to twin-boundary orientations. The downturn toward zero resistivity at the shoulder is indicated by the solid arrow. In the inset the normalized resistivity is plotted vs reduced temperature for crystals Y0a, Y90, and DT2 with $\mathbf{H} = 2$ T $\|c$. The open arrows indicate temperatures at which the angular scans shown in Fig. 13 were taken. The solid arrows and dashed line illustrate the difference in normalized resistivity between the twinned crystals and the detwinned crystal DT2, which is a relative measure of the effect of TB pinning at a given temperature.

A. Onset of twin-boundary pinning

Figure 4 displays the angular dependence of the resistance of crystal Y0b ($F_L \perp$TB) for a resultant magnetic field of 3 T rotated in the plane perpendicular to the TB's and taken at fixed temperature intervals of ~ 0.2 K in the temperature regime below the shoulder. At low temperatures the resistance is found to increase as the magnetic field is tilted away from the TB's (and the c axis), eventually reaching a maximum, and then decreases as dictated by the anisotropy of the system upon further rotation toward the ab plane. As in our earlier study for magnetic fields in the ab plane, TB pinning manifests itself as a drop in the resistivity when the magnetic field is oriented within some angular width about the TB's.[15] We operationally define the depinning angle θ_p as half of the angular width between resistance maxima (see Fig. 9). A depinning angle of $\theta_p \sim 19°$ is observed for temperatures within ~ 0.5 K of the zero-resistance temperature. The pinning drop becomes less dramatic as the temperature is increased and eventually disappears near 87.25 K. The top panel of Fig. 5 shows the higher-temperature curves like those in the preceding figure at a finer temperature interval of 0.1 K. Vestiges of TB pinning are detectable up to 87.25 K, but cannot be discerned at 87.35 K. Thus the onset temperature (T_{TB}) below which TB pinning causes a drop in the angular-dependent magnetoresistance curve for $\mathbf{H}=3$ T can be identified as 87.30 ± 0.05 K.

To correlate the temperature at which the downturn in the resistive transition occurs with T_{TB}, a well-defined point characterizing the shoulder must be established. The resistive transition and its temperature derivative for $\mathbf{H}=3$ T $\|c$ are shown in the bottom panel of Fig. 5. The resistance is approximately linear over a small temperature interval of approximately 1 K (87.40–88.40 K) just above the downturn. The derivative features a relatively constant value of ~ 3 mΩ/K over this temperature range before a steep upturn at ~ 87.40 K (marked by the solid arrow) reflecting the change in curvature associated with the downturn in the resistive transition. Points marking the upturn in the derivative, and henceforth denoted by

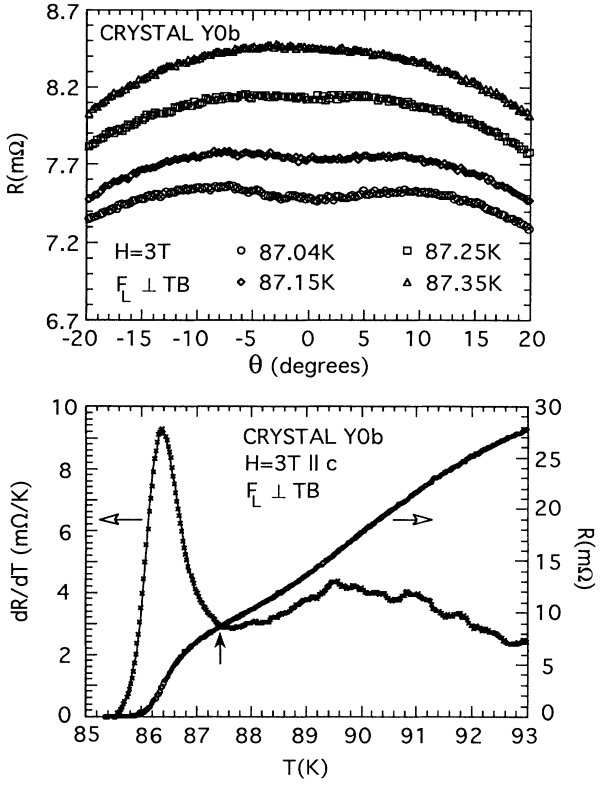

FIG. 5. Similar curves to those presented in the preceding figure are exhibited in the top panel except at a finer temperature interval of 0.1 K near the onset of TB pinning. Vestiges of pinning are distinguishable up to 87.25 K, but are not identifiable at 87.35 K. The resistive transition and its temperature derivative for $\mathbf{H}=3$ T $\|c$ are displayed in the bottom panel. The point T_{sh} marking the steep upturn in the derivative (solid arrow) is chosen to represent the shoulder in the resistive transition.

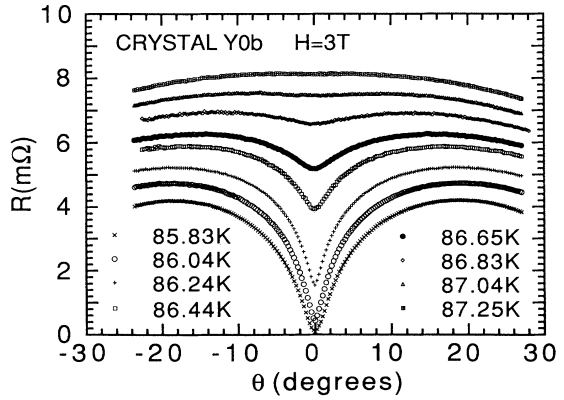

FIG. 4. Effect of TB pinning on the angular dependence of the magnetoresistance is displayed for rotation of a resultant magnetic field of 3 T off the c axis. The curves were taken at fixed temperature approximately every 0.2 K.

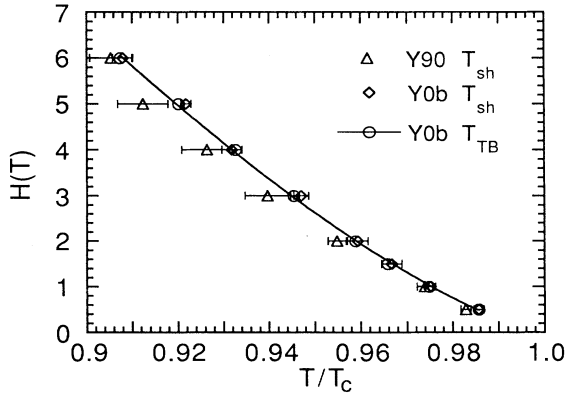

FIG. 6. Onset temperatures for TB pinning T_{TB} and T_{sh} as defined in the previous figure are plotted vs magnetic field. The solid curve is a fit to the equation $\mathbf{H}=\mathbf{H}_0(1-T_{TB}/T_c)^n$ with the values $\mathbf{H}_0=153$ T and $n=1.36$.

T_{sh}, were chosen to represent the shoulder in the resistive transition. Plotted in Fig. 6 are the points T_{sh} and the onset temperature T_{TB} for Y0b as a function of magnetic field. The onset temperature T_{TB} and the T_{sh} points are clearly correlated, indicating that the shoulder is a manifestation of TB pinning. The line is a fitted curve of the form $\mathbf{H}_0(1-T_{TB}/T_c)^n$, with $n=1.36$ and $\mathbf{H}_0=153$. In addition, we present the T_{sh} points for crystal Y90 to emphasize that the shoulder occurs essentially at the same reduced temperature for a given field regardless of the crystal or Lorentz-force configuration. We estimate the temperature uncertainty of T_{sh} for crystal Y0b to range from ~ 0.2 to 0.5 K with increasing magnetic field due to "noise" in the derivative. It is more difficult to distinguish T_{sh} when the downturn is less pronounced, leading to larger uncertainty for Y90 (up to 1 K for the highest magnetic fields measured).

As an alternative determination of the TB-pinning onset temperature, the deviation point of the normalized resistive transitions for a twinned crystal and a detwinned crystal with similar high-temperature behavior might be taken. We make such a comparison in Fig. 7 in which the normalized resistivity versus reduced temperature for crystal Y0b and a "clean" detwinned crystal DT1 for $\mathbf{H}=3$ T $\|c$ is shown. The agreement of the temperature dependences of the two crystals at high reduced temperatures is excellent with the deviation point of the two curves, indicated by the open arrow, occurring at $T/T_c \sim 0.955$ near the onset of the linear region just above the shoulder. This deviation point corresponds to $T=88.13$ K for crystal Y0b, which is ~ 0.8 K above the measured T_{TB} for this magnetic field. Thus it is possible that TB pinning persists to temperatures slightly above T_{TB} and acts to suppress or flatten the angular-dependent background in the highest-temperature $R(\theta)$ curve of Fig. 5 without producing a well-defined pinning dip. However, it is clear that by either of the criteria we have chosen, the onset of TB pinning occurs within 1 K of the shoulder marking the downturn to zero resistance.

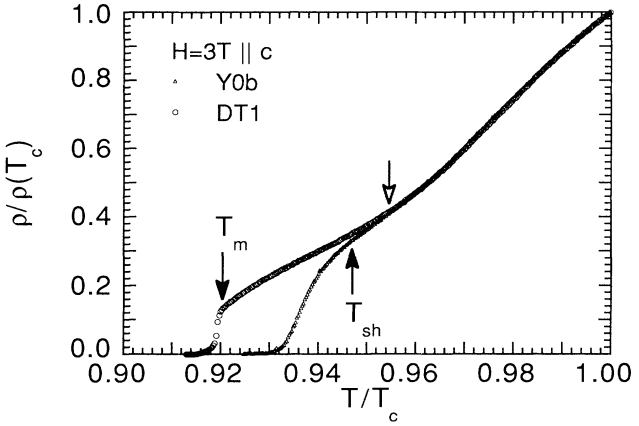

FIG. 7. Normalized resistive transitions for the detwinned crystal DT1 and the twinned crystal Y0b coincide down to $T/T_c \sim 0.955$ (open arrow) corresponding to $T \sim 88.13$ K for Y0b. This point of deviation can be taken as an alternative measure of the TB-pinning onset temperature. The flux-lattice melting transition for DT1 and the shoulder for Y0b are indicated by T_m and T_{sh}, respectively.

The sharp kink exhibited for DT1 at $T/T_c \sim 0.92$ labeled by T_m, below which non-Ohmic I-V characteristics were observed,[12] is distinct from the smooth shoulder with Ohmic resistivity exhibited by Y0b. The presence of the sharp kink which we associate with flux-lattice melting is observed in "clean" crystals characterized by high transition temperatures $T_c > 92$ K and narrow transition widths $T_c \leq 0.3$ K.[12] An angular scan centered on the c axis for $\mathbf{H}=4$ T at a temperature below the shoulder and near the zero-resistance point of crystal Y0b is shown in the top panel of Fig. 8. The temperature 87.65 K ($T/T_c \sim 0.916$) was chosen such that it was low enough to observe strong pinning by the TB's (as evidenced by the large pinning dip), but high enough to obtain the current-voltage characteristics over two orders of magnitude. The lower panel of the same figure shows the I-V curves measured for $\mathbf{H}\|c\|$TB and with the magnetic field oriented 20° off the c axis. In both cases the I-V curves are linear with slopes of unity and Ohmic behavior is observed within our resolution.

B. Lorentz-force dependence of twin-boundary pinning

The angular dependence of the resistivity of crystals Y90 ($F_L \|$ TB) and Y0a ($F_L \perp$ TB) for a resultant magnetic

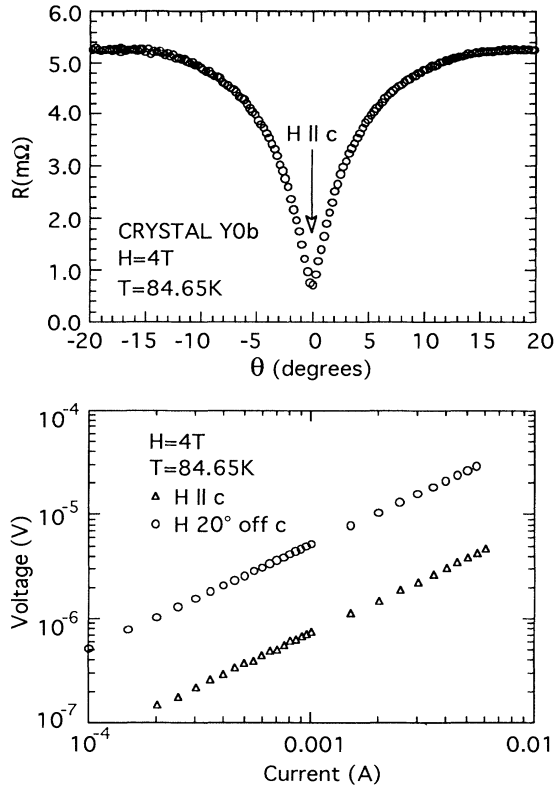

FIG. 8. Top panel is a representative TB-pinning curve for a 4-T magnetic field rotated off the c axis at $T=84.65$ K. The bottom panel shows on a logarithmic plot the current-voltage characteristics taken for $\mathbf{H}\|c$ and with the magnetic field directed at 20° off the c axis at the same temperature.

field of 2 T rotated in the plane containing the c axis and the TB normal is shown in Fig. 9. Two striking differences between the two curves are immediately identifiable: (1) The depinning angle measured for crystal Y0a is more than twice that of crystal Y90, and (2) the ratio $\rho(\theta_p)/\rho(0°)$ is two orders of magnitude larger for crystal Y0a than crystal Y90. For both crystals Y0a and Y0b with $F_L \perp$TB, we observed the largest depinning angles, up to 24° at 1 T, accompanied by the most pronounced pinning dips. Twin-boundary pinning manifests itself over larger angles in our measurements than those observed in torque measurements ($\sim 5°-7°$) at lower temperatures (77 K).[27] Decoration experiments reveal that the TB's affect the vortex configuration for tilts up to $\sim 40°$ off the c axis in low magnetic field (10 Oe) and liquid-helium temperatures.[30]

The data exhibited in Fig. 9 were taken at a fixed temperature, and ideally one might expect comparing data taken at the same reduced temperature would allow quantitative comparison of the results for the two configurations. However, TB pinning for Y90 only becomes appreciable at reduced temperatures which are below the zero-resistance point of crystal Y0a as revealed by a comparison for these two crystals of the field-broadened resistive transition for $\mathbf{H}=2$ T $\|c$. Shown in the inset of Fig. 3 are the normalized resistive transitions for crystals Y0a and Y90 and additional data taken on a "dirty" detwinned crystal DT2 for the temperature regime around the shoulder. The weak shoulder for crystal Y90, associated with the onset of TB pinning, is observed to occur at a reduced temperature ($T/T_c \sim 0.949$) in the vicinity of the zero-resistance temperature for crystal Y0a, and thus it is not possible to investigate TB pinning at the same reduced temperature and magnetic field for the two crystals. Alternatively, we have chosen to compare temperatures for which the resistivities with $\mathbf{H}\|c$ for the two crystals are approximately the same fraction ($\sim 1\%$) of their respective resistivities at T_c.

Comparison of the resistive transitions of Y0a and Y90 with that of the DT2 yields insight into the size difference of the pinning maxima exhibited in Fig. 9 for the two twinned crystals. The drop in resistivity due to TB pinning is just the difference $R(\theta_p)-R(0°)$. At θ_p the angular-dependent vortex pinning by the TB's can no longer be distinguished from the background due to point-defect pinning, and $R(T,\theta_p)$ for the twinned crystals can be approximated by that for the detwinned crystal. For a qualitative description, we shall compare the resistive transitions of the twinned crystals with $R(T,0°)$ of DT2 rather than $R(T,\theta_p)$ since our conclusions are not altered by this approximation (see Fig. 13 for the angular dependence of DT2). The relative size of the pinning dip for a given twinned crystal can thus be reconstructed by taking the difference between its resistive transition and that of DT2 as indicated by the solid arrows in the inset of Fig. 3. The difference between the normalized resistivities of Y90 and DT2 are much smaller than those for Y0a and DT2 for all reduced temperatures not too close to their respective shoulders, and thus Y0a exhibits a larger pinning dip. The relative size of the pinning dip for Y0a constructed in this manner decreases substantially and monotonically as the temperature is increased as is verified in temperature-dependent studies of the TB-pinning curves such as those shown in Fig. 4. In comparison, the pinning dip for Y90 exhibits weak but nonmonotonic behavior as we have observed by temperature-dependent studies of the TB-pinning curves for this crystal (see Fig. 3 of Ref. 35).

The TB-pinning curves for crystal Y0a as a function of magnetic field are shown in Fig. 10. The curves were taken at temperatures to achieve the 1% resistivity criterion for the orientation $\mathbf{H}\|c\|$TB as described above. The de-

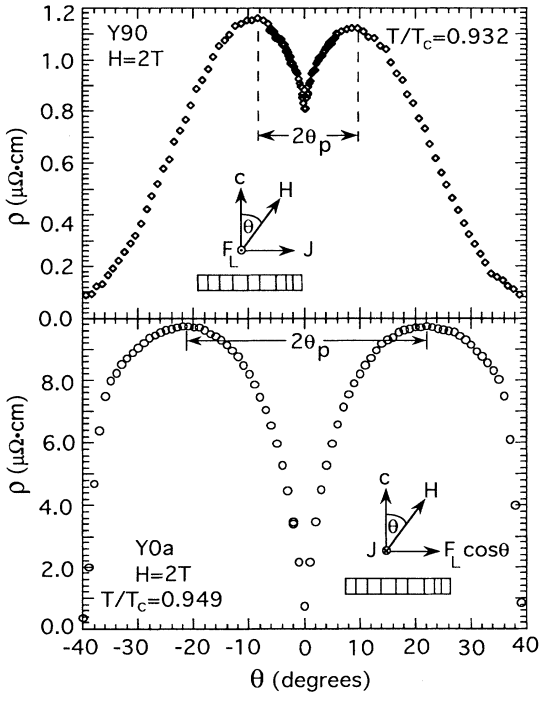

FIG. 9. Angular dependence of the resistivity for rotation of a magnetic field of 2 T off the c axis for crystals Y90 (upper panel) and Y0a (lower panel). The depinning angle θ_p is defined as half of the angular width between resistance maxima. The insets show the experimental configuration for each crystal.

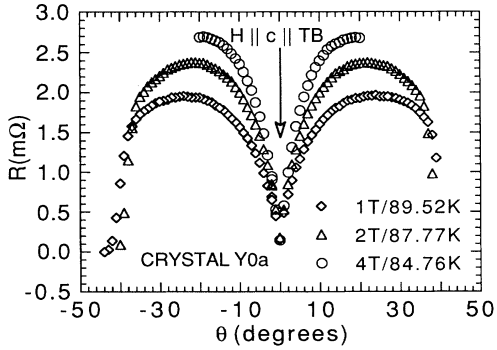

FIG. 10. Magnetic-field dependence of the TB-pinning curves of crystal Y0a for rotations off the c axis is displayed. Each curve was taken at a temperature such that the resistivity for $\mathbf{H}\|c\|$TB was 1% of the resistivity at T_c.

pinning angle is found to be magnetic-field dependent, decreasing smoothly with increasing magnetic field and lower temperature. The magnitude of the pinning maxima is observed to increase with magnetic field. We note that it is difficult to extract the true magnetic-field dependence of the shape of the pinning curves and the associated depinning angle since TB pinning occurs at different temperatures for different values of the magnetic field and thus temperature effects are unavoidable.

A summary of the values of the depinning angles obtained for the various Lorentz-force configurations versus magnetic field is presented in Fig. 11. For all but one of the crystals, θ_p was found to decrease smoothly with magnetic field over the entire range investigated. The magnetic-field behavior of θ_p for crystals Y90 and Y0a is almost linear with fitted slopes of $-1.3°/T$ and $-1.6°/T$, respectively. For crystal Y0b the depinning angle decreases quite rapidly with field at low magnetic fields and saturates at a value of $\sim 19°$ for fields above 2 T. From a comparison of the depinning angle of these crystals for a given magnetic field, θ_p is found to increase monotonically with the angle between the Lorentz force and the TB's. We believe that this increase of θ_p corresponds to an enhancement of the pinning barriers and results in different dynamical situations for the various flux-motion directions as will be discussed in Sec. III D. These enhanced pinning barriers cause the steeper downturn toward zero resistance at the shoulder in the resistive transitions when $F_L \perp$TB as displayed in Fig. 3 and the associated pronounced pinning cusp observed in Figs. 4 and 9.

To assure that the features observed in the angular dependence of the resistance are due to the TB's, we made the following checks. First, for several crystals the magnetic field was not only tilted out of the TB's, but also rotated in the TB plane. Figure 12 shows the angular dependence for both types of rotation for crystal Y0a in a magnetic field of 2 T. The top curve for the magnetic field rotated out of the TB's is identical to that presented in the bottom panel of Fig. 9. A logarithmic scale is chosen for the vertical axis to emphasize the absence of a pinning dip when the magnetic field is rotated in the TB's (lower curve). The resistance is found to be lower when

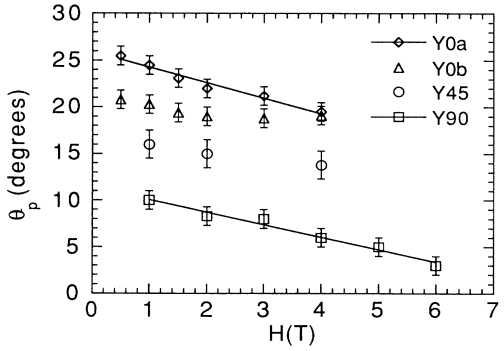

FIG. 11. Depinning angle (θ_p) vs magnetic field is plotted for all four twinned crystals. The straight lines are linear fits to the data for Y0a and Y90 with slopes of $-1.6°/T$ and $-1.3°/T$, respectively. The depinning angle shows a monotonic increase as the angle between the Lorentz force and the TB's increases.

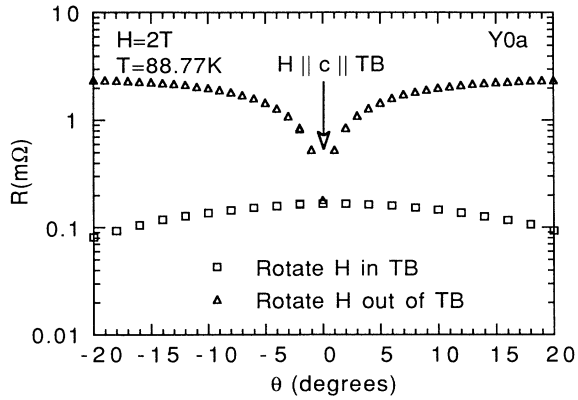

FIG. 12. Angular dependence of the resistance of crystal Y0a for rotation of a 2-T magnetic field off the c axis in the TB's (squares) and normal to the TB's (triangles).

the magnetic field is confined to the twin-boundary plane and falls off monotonically as the tilt angle increases. We interpret these results as indicating that vortices are pinned regardless of the angle as long as the magnetic field is parallel to the TB's and that the angular dependence is determined by the superconducting anisotropy of the system.

Additionally, the angular dependence of the magnetoresistance about the c axis of the detwinned crystal DT2 was measured for various temperatures near the zero-resistance point for $\mathbf{H}=2$ T (see Fig. 13). In contrast to the behavior exhibited by twinned crystals, no evidence of a pinning minimum is observed; rather, the resistance is found to decrease uniformly as the magnetic field is rotated off the c axis. The corresponding reduced temperatures at which these angular scans were taken are indicated by open arrows in the inset of Fig. 3. The distinct downturn associated with the onset of TB pinning is not observed in the field-broadened transitions of this crystal as is evident in the inset of Fig. 3. Consequently, the zero-resistance point for $\mathbf{H}=2$ T $\|c$ occurs at a re-

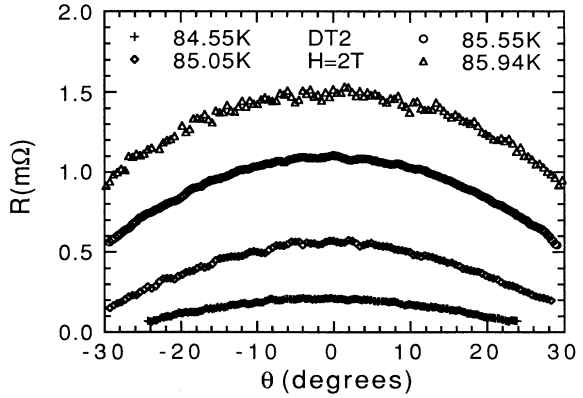

FIG. 13. Angular dependence of the resistance of the detwinned crystal DT2 for various temperatures and a 2-T magnetic field rotated off the c axis. No drop in the resistance associated with TB pinning is observed when the magnetic field is nearly aligned with the c axis.

duced temperature $T/T_c \sim 0.924$ slightly lower than that for crystal Y90.

The absence of the melting kink (see T_m in Fig. 7) in the resistive transition for DT2 in addition to its poorer zero-field characteristics lead us to believe that this crystal contains more defects than DT1 and hence the label "dirty." In contrast to the high transition temperature and narrow transition width of the "clean" crystal DT1, this crystal had a $T_c \sim 90.83$ K and a broader transition width $\Delta T_c \sim 0.45$ K due presumably to a larger number of oxygen vacancies. Apparently, these types of defects introduce more disorder into the Abrikosov lattice and suppress the melting transition. We note the qualitative similarity in appearance of the field-broadened transitions of crystals Y90 and DT2 with $\mathbf{H}=2$ T $\|c$ in the inset of Fig. 3, which suggests that the mechanism for dissipation when $F_L \| \mathrm{TB}$ might be flux motion along a direction with enhanced point-defect pinning.

C. Crystallographic anisotropy

The current configuration relative to the TB's of Y90 provided the unique opportunity to investigate the crystallographic anisotropy of TB pinning since for both orientations $\mathbf{H}\|c\|\mathrm{TB}$ and $\mathbf{H}\|ab\|\mathrm{TB}$ the maximum Lorentz force is achieved ($\mathbf{H}\perp J$). We present in Fig. 14 a normalized angular-dependent resistance for convenience of comparison of θ_p for 1 and 4 T for the two orientations. The residual resistance for $\mathbf{H}\|\mathrm{TB}$ has been subtracted out from the raw data (see, for example, Fig. 16 or Ref. 35), and the remainder has been normalized to the maximum value at the depinning angle, i.e., $[R(\theta)-R(0°)]/[R(\theta_p)-R(0°)]$. The depinning angle for field rotations off the c axis (top panel of Fig. 14) was found to decrease systematically with increasing magnetic field from 10° at 1 T to 6° at 4 T in an approximately linear fashion (see Fig. 10). In contrast, there was no magnetic-field dependence of θ_p detected within our resolution for field rotations in the ab plane (bottom panel of Fig. 14). Furthermore, for $\mathbf{H}<4$ T the depinning angle for tilts about the c axis is greater than that for rotations in the ab plane.

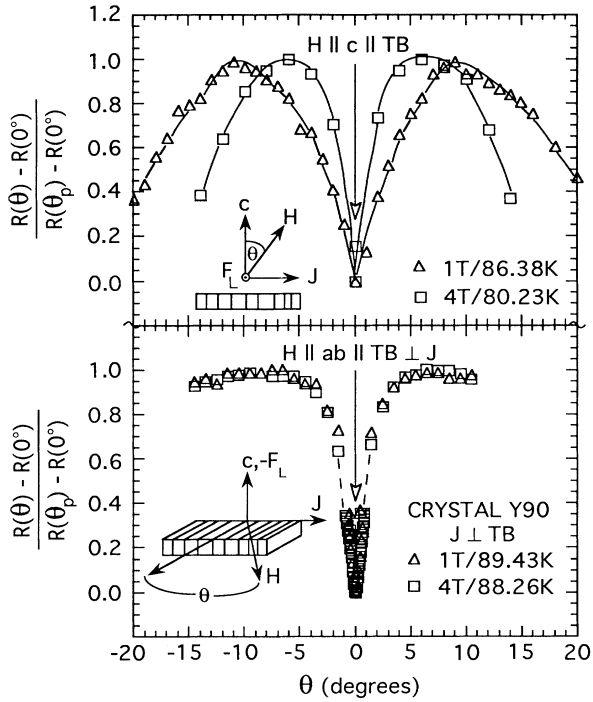

FIG. 14. Angular dependence of the normalized resistance of crystal Y90 ($J\perp$TB) for magnetic fields of 1 and 4 T rotated off the c axis (top panel) and rotated about the TB's in the ab plane (bottom panel). The lines through the data are a guide to the eye. The insets show the experimental configuration.

Note that the pinning curves were obtained at different temperatures. The field-broadened resistive transitions and the zero-resistance points differ substantially for the two field orientations (see, for example, Refs. 1 and 2), and hence it is not possible to compare TB-pinning curves at the same temperature for reasonably large magnetic fields. However, as can be seen in Fig. 4, at very low resistivity levels for $\mathbf{H}\|c$ (i.e., temperatures in the immediate vicinity of the zero-resistance point) θ_p does not change dramatically with temperature or, equivalently, with the resistivity criterion. Consequently, the temperatures were chosen to obtain a resistivity as close as possible to 1% of $\rho(T_c)$ when the field was aligned with the TB's. Although the depinning angle is not temperature dependent in this range, the height of the resistance maximum, i.e., $R(\theta_p)-R(0°)$, is highly sensitive to temperature and the resistivity-level criterion. However, we note that the pinning maxima are more pronounced for rotations in the ab plane than for those off the c axis for all temperatures well below their respective pinning onset temperatures T_{TB} (see Fig. 15 for an example of the raw data when the magnetic field is rotated in the ab plane).

The observed difference in behavior for the two orientations may be due to several factors. The tilt modulus for rotations in the ab plane is predicted to be larger than that for rotations off the c axis by a factor of $\Gamma^{1/2}$, where Γ is the mass anisotropy m_c/m_{ab}.[21,36,37] Thus the vortices are more resilient to bending when tilted in the ab plane causing a smaller depinning angle. In addition, this process may be affected by the intrinsic pinning mechanism when the magnetic field is rotated in the ab plane, the onset of which we have previously shown to occur at a temperature above T_{TB}.[33] There may also be effects due to different measurement temperatures. We have previously found the pinning behavior for the two axes of rotation to be dramatically different for low oxygen contents. Twin-boundary pinning was shown to be relatively insensitive to large changes in the stoichiometry for rotations in the ab plane, whereas for rotations off the c axis TB pinning was not observed.[34]

D. Vortex dynamics in the presence of twin boundaries

The existence of sharp drops in the angular-dependent magnetoresistance for tilt angles less than θ_p off the TB's implies that the vortices are pinned in the TB's over some part of their length for these field orientations. The static configuration of the pinned-vortex structure (obtained in the zero-current limit) should be identical for the crystals

Y0a, Y0b, and Y90 since the tilt direction with respect to the TB's is the same for rotations off the c axis. Therefore, if the static configuration is not perturbed too greatly by the driving force, then the observed difference in the pinning boundary for the two Lorentz-force orientations must be due to different dynamical situations. In crystals Y0a and Y0b, the dominant component of the Lorentz force is normal to the TB's, and thus the large potential barriers associated with the planar interface of the TB must be overcome. These barriers are due to the strain field associated with the interchange of the a and b axes across the twin plane and are present even when the TB's are free of atomic defects. For crystal Y90 the Lorentz force is along the TB's and we may consider the qualitatively different case of motion impeded by point-defect pinning which is likely to be enhanced in the TB's relative to the bulk. For such a case, it should be possible to reproduce our transport results with the appropriate assumptions about the relative magnitude of the friction coefficients in the TB's and the bulk.

The static configuration of a single vortex for a magnetic field oriented at an arbitrary angle relative to the TB's was considered in a model proposed by Blatter, Rhyner, and Vinokur.[31] The vortex configuration is determined by two competing energy contributions: (1) $\Delta\varepsilon$, the gain in energy due to pinning by TB's, and (2) the cost of elastic energy of bending the vortex away from the internal magnetic field. When the magnetic field is parallel to the TB's, the vortex is straight and pinned over its entire length. The model assumes that for small misalignments the vortex adjusts itself such that some segments of the vortex remain in the TB's to take advantage of the reduced (condensation) energy. The resulting vortex is "kinked" into segments of length $r(\theta)$ lying within the TB's joined by others of length s traversing the regions between neighboring TB's [see inset (b) of Fig. 15]. As the magnetic field is further rotated away from the TB's, the deviation of the adjusted vortex from the internal magnetic field becomes more pronounced, and an increasing cost of elastic energy is accompanied by a continuous reduction of the length $r(\theta)$ of the segments pinned in the TB's. The critical angle θ_c is defined as the angle at which $r(\theta)$ goes to zero and occurs when the elastic energy exactly compensates the pinning energy, i.e., in the small-angle approximation $\theta_c=(2\Delta\varepsilon/\varepsilon_l)^{1/2}$, where ε_l is the tilt modulus of an isolated vortex. Throughout the tilting process, the outlying segments traversing the domains between TB's have both a constant length s and a fixed orientation of θ_c from the TB's. Above the critical angle, the cost of elastic energy becomes so great that it is no longer energetically favorable for the vortex to bend and the vortex is directed parallel to the internal magnetic field. A similar model has been used to interpret the angular dependence of TB pinning for low magnetic field (~ 10 Oe) and low temperature (4.2 K) as determined by decoration techniques.[30] In what follows we neglect nonlocal effects in an attempt to describe qualitatively our data.

Our resistive measurements are carried out in a situation far from static. However, one could imagine that in the case where the vortices are driven parallel to the TB's (as in Y90) the actual configuration of moving vortices does not differ from the static one, and the ideas of Ref. 31 can be applied to the dynamics in order to describe the behavior of the resistivity qualitatively. If the vortex moves along the TB's preserving its static kinked configuration, the friction force per unit length on the part of the vortex confined between two neighboring TB's, comprised of the segments r and s, can be written as

$$f=\frac{f_{\mathrm{TB}}r(\theta)+f_b s}{r(\theta)+s} ,$$

where f_{TB} and f_b are the friction forces per unit length in the TB and the bulk when $\theta=\theta_c$, respectively. Since the resistivity is inversely proportional to the friction, this gives rise to an angular-dependent resistivity

$$\rho(\theta)=\rho_{\mathrm{TB}}\frac{r(\theta)+s}{r(\theta)+(\rho_{\mathrm{TB}}/\rho_b)s} ,$$

where ρ_{TB} is the resistivity associated with flux motion in the TB's and ρ_b is the corresponding resistivity for flux motion in the bulk when $\theta=\theta_c$. We have solved for $r(\theta)$, s, and θ_c exactly using the general approach of Ref. 31 to extend the range of validity beyond the small-angle approximation. These exact expressions for $r(\theta)$, s, and θ_c, with the assumption that our operationally defined depinning angle is a measure of the critical angle ($\theta_p\approx\theta_c$), can be substituted into the above equation for $\rho(\theta)$. The values of ρ_{TB} and ρ_b can be obtained from the experimental data such as from the top panel of Fig. 9 for $\theta=0°$ and θ_p, respectively. The simplest orientation to try to fit is for field rotations in the ab plane for which the angular-dependent background is understood quantitatively to

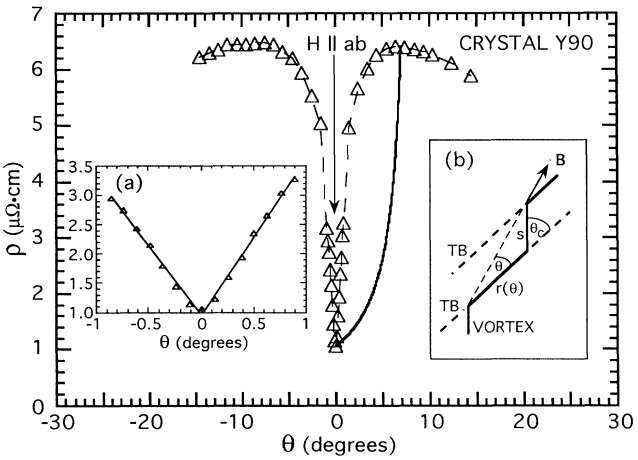

FIG. 15. Angular dependence of the resistivity for a 1-T magnetic field rotated in the ab plane. The solid curve is obtained from the expression for $\rho(\theta)$ in the text with the experimental values $\rho_{\mathrm{TB}}=1.07$ $\mu\Omega$ cm, $\rho_b=6.44$ $\mu\Omega$ cm, and $\theta_c=7°$. The expression for $\rho(\theta)$ is an even function of θ, and we present the curve generated only for $\theta>0$. Inset (a) shows the low-angle data with the least-squares-fitted lines yielding an average slope $|d\rho/d\theta|_0\sim 2.5$ $\mu\Omega$ cm/deg. Inset (b) exhibits the kinked vortex structure of Ref. 31 with the lengths $r(\theta)$ and s defined.

vary as $\cos^2\theta$ as a result of Lorentz-force-induced dissipation. For the small angular range over which the TB's are effective in pinning ($\theta_p \approx 7°$), this background is essentially constant. Thus the above expression for $\rho(\theta)$ should account for the observed shape of the pinning curves, if a simple extension of the static configuration is appropriate to describe the dynamics. In the main part of Fig. 15 we show the angular dependence of the resistivity at a fixed temperature of 89.43 K and for a magnetic field of 1 T confined to the *ab* plane. The solid curve shows the angular dependence obtained from the above expression for $\rho(\theta)$ with the values $\rho_{\rm TB}$, ρ_b, and $\theta_c \approx 7°$ taken from the data. Although quite naturally we find the resistivity to increase as a function of angle, the curvature of $\rho(\theta)$ is positive over almost the entire angular range below θ_p in contrast to our data. Furthermore, the predicted $\rho(\theta)$ is a much more slowly changing function of angle than the observed behavior. A small-angle expansion of $\rho(\theta)$ about $\theta=0$ yields the relation

$$\theta_c = \rho_{\rm TB}\left[1+\frac{\rho_{\rm TB}}{\rho_b}\right]\left[\frac{d\rho_{\rm TB}}{d\theta}\right]_0^{-1},$$

from which we can calculate the expected value of θ_c from the initial value of the slope of $\rho(\theta)$ and the values of $\rho_{\rm TB}$ and ρ_b. The low-angle data ($|\theta| < 1°$) are shown in inset (a) of Fig. 15. The lines are least-squares fits to the data, giving an average initial slope of $|d\rho/d\theta|_0 \sim 2.5$ $\mu\Omega$ cm/deg. With this slope we obtain a value $\theta_c \sim 0.35°$, which is an order of magnitude smaller than the range over which we observe TB pinning. We obtain a similar value of $\theta_c \sim 0.36°$ for the 4-T data and the same magnetic-field orientation. The dynamics with the magnetic field oriented parallel to the *ab* plane and the Lorentz force normal to the CuO_2 planes may be complicated by the intrinsic pinning mechanism and lead to the disparity between theory and our results. Although in the absence of intrinsic pinning for rotation of a 2-T magnetic field off the *c* axis we obtain a more reasonable value of $\theta_c \sim 2°$ in the same manner, the curvature predicted by the model remains incorrect. It appears that the static configuration predicted by Blatter, Rhyner, and Vinokur[31] is not preserved in the high-temperature regime of our dynamic experimental results. It is possible that the smearing of the pinning potential by thermal fluctuations provides only a small perturbation on the dynamics. However, our results show that even at these high temperatures the TB's produce a substantial effect on the resistivity.

Many of the previous measurements of the field-broadened resistive transition in the literature have been interpreted in terms of thermally activated flux motion through pinning barriers at temperatures below the shoulder.[1,2] Such data suggest indirectly that at the shoulder the vortex structure undergoes a crossover from an unpinned state to a state in which pinning becomes effective and activated behavior is observed. Our measurements show directly that below the shoulder pinning becomes effective in impeding motion of the vortex structure and that for magnetic fields precisely aligned with the *c* axis the TB's are the predominant pinning centers giving rise to the shoulder. The question of why TB pinning turns on at this particular temperature remains open. Worthington, Holtzberg, and Feild[13] have suggested that the shoulder might indicate a phase boundary between the isotropic and hexatic liquid states predicted by Marchetti and Nelson.[5] Formation of a hexatic liquid of entangled flux lines at lower temperatures gives rise to an enhanced viscosity due to the torsional rigidity associated with preserving orientational order. This phase transition is an intrinsic property of the vortex structure and occurs in the absence of pinning. However, the consequences of pinning by macroscopic inhomogeneities such as TB's can be transmitted over large length scales in such a state and have a dramatic effect on restricting flux motion.[6] An alternative view proposed by Vinokur *et al.* interprets the shoulder as the smooth crossover from an unpinned liquid at temperatures above the shoulder to a pinned liquid at lower temperatures, which occurs only in the presence of disorder and large barriers for the plastic motion of vortices.[4] These liquid theories can be distinguished by their predicted temperature dependences for the friction coefficient γ and intervortex viscosity η of the vortex fluid.[38] Quantitative comparison with any theoretical model requires a relatively uniform twin density since the calculated resistivity for the Lorentz-force configuration of Y90 depends exponentially on the TB spacing.[6] We are currently investigating the possibility of measuring the two hydrodynamic parameters on the same crystal.

E. Evolution of the melting kink

The existence of sharp pinning dips in the angular dependence of resistance provides a reference for alignment of the magnetic field with the *c* axis, and the angular resolution of the crossed magnetic-field technique allows for precise alignment. In the top panel of Fig. 16, the region around the downturn in the resistive transition of crystal Y0b is displayed for a resultant magnetic field of 2 T oriented between 0° and 10° off the *c* axis at 2.5° intervals. The transition curves coincide above the shoulder (marked by the solid arrow), but deviate below it as the resistance for a given temperature shifts to higher values with increasing angle and the downturn becomes less pronounced. For the 10° misalignment, the downturn in the transition curve at ~88.20 K is barely identifiable. The zero-resistance point shifts to a lower temperature ~86.90 K for the off-axis orientations, but is relatively insensitive to the degree of misalignment. In addition, a second kink in the transition curve, indicated by the open arrow, develops at $T \sim 87.05$ K, very close to the zero-resistance point. This kink is barely observable at 2.5° and is clearly distinguishable at larger angles. Analogous curves for larger angles are exhibited in the lower panel of Fig. 16, which shows that the zero-resistance point gradually moves to higher temperature and at the high-temperature end the resistance decreasing slightly with increasing angle. These results indicate that at angles larger than 10° the intrinsic anisotropy starts to manifest itself. The curves cross each other at ~88.15 K, which is near the temperature at which the shoulder

occurs at lower angles. This crossover is due to competing effects of the anisotropy reducing the resistance at higher angles and the TB's reducing the resistance for lower angles at temperatures below 88.15 K. The angular scans for TB pinning were taken at constant temperature just above the zero-resistance point for $\mathbf{H}\|c\|\mathrm{TB}$ (0°) and can be reconstructed by following an isotherm such as the one depicted (dashed line) in Fig. 16 at 87.60 K. Initially, the resistance increases dramatically with angle until a plateau is reached at ~17.5°, and upon further rotation of the field the resistance decreases gradually.

We have followed the evolution of the second kink as the magnetic field is rotated toward the *ab* plane. At a misalignment as low as 7.5°, the kink is found to delineate a non-Ohmic regime at low temperatures from an Ohmic regime at high temperatures as demonstrated in Fig. 17. The top panel displays that the *I-V* curve is linear at a temperature 87.07 K just above the kink, but is nonlinear at a temperature 86.95 K slightly below it. The low-temperature end of the transition is shown in the lower panel with corresponding temperatures at which the *I-V* curves were taken indicated by arrows. At angles smaller than the depinning angle, there is an interplay between TB pinning and the transition to non-Ohmic behavior. This transition is completely suppressed for the magnetic field exactly aligned with the TB's. It has been suggested that at low angles this transition may be a manifestation of Bose glass behavior due to the correlated disorder of the TB's (Refs. 12 and 39) and that such behavior might be the cause of the previously observed cusplike behavior in the angular dependence of the peak in the resistive component of the ac susceptibility (χ'').[40] An experimental check of whether the *I-V* curves in the transition region obey the predicted dynamical scaling laws[39] is required to make more definitive statements about the nature of the transition for angles less than θ_p, and such experiments are being considered. For angles above the depinning angle, we have shown the kink temperature to obey the angular dependence expected for flux-lattice melting.[12] The similarity between "clean" twinned and detwinned crystals for the magnetic field oriented at an angle larger than θ_p is demonstrated in Fig. 18, in which we show the normalized resistive transition of crystal Y0b along with that of crystal DT1 for a misalignment of 30° off the *c* axis. The salient features of the curves are similar with the melting kink occurring at approximately the same reduced temperature and value of the normalized resistivity (~12%). The normalized resistivity of the twinned crystal is slightly lower than that of the detwinned crystal at temperatures immediately above the melting transition. This may be due to

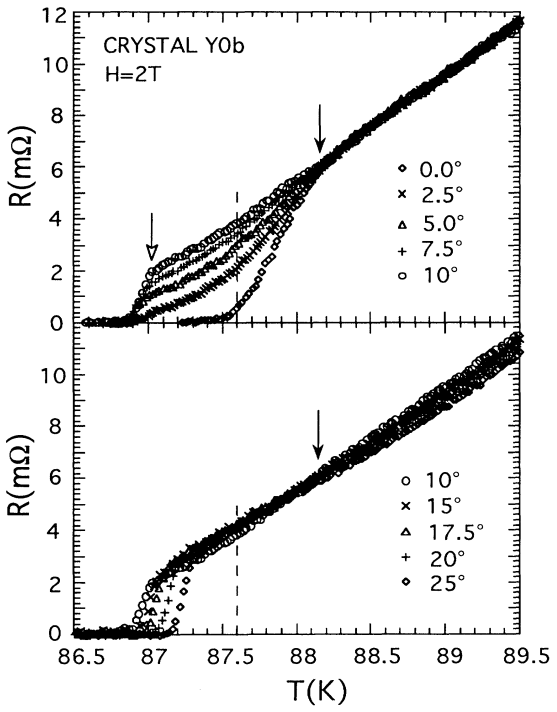

FIG. 16. Low-temperature end of the resistive transitions of crystal Y0b is displayed to emphasize the region around the shoulder (solid arrow) for various orientations of a 2-T magnetic field with respect to the *c* axis. The top panel shows the transitions at 2.5° intervals up to a 10° misalignment. The bottom panel shows the transitions at larger misalignments. A pinning curve can be reconstructed by following an isotherm such as the dashed line at 87.60 K with increasing angle.

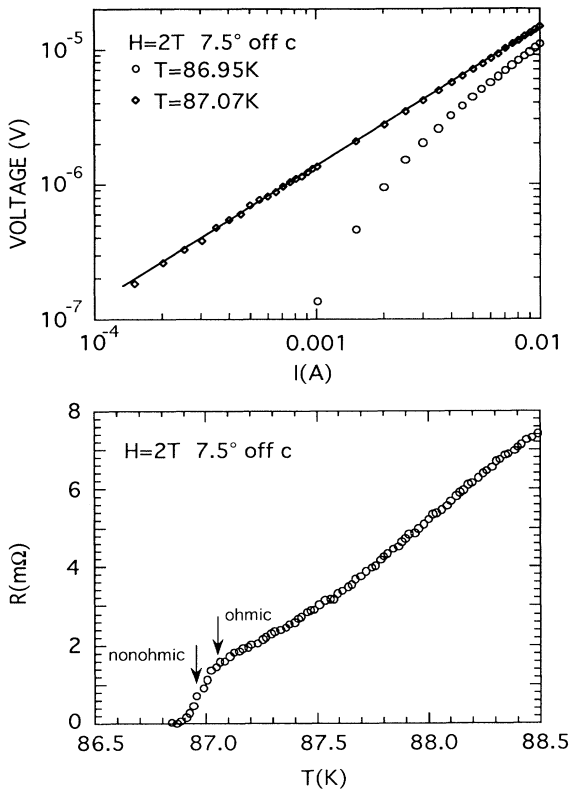

FIG. 17. Top panel shows *I-V* curves taken with a magnetic field of 2 T oriented 7.5° off the *c* axis and at temperatures just above ($T=87.07$ K) and below ($T=86.95$ K) the kink observed in the resistive transition. The bottom panel shows the relation of these temperatures to the kink in the resistive transition. The kink is found to mark the onset of nonlinear behavior.

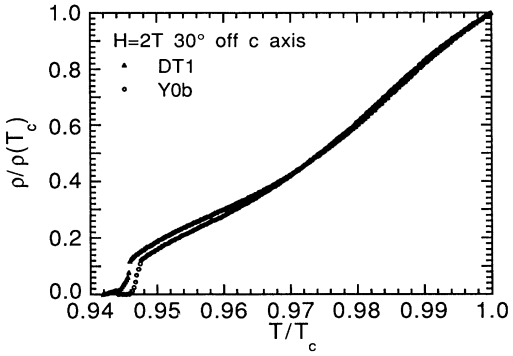

FIG. 18. Normalized resistive transitions are shown for the detwinned crystal DT1 and the twinned crystal Y0b for a magnetic field of 2 T tilted 30° off the c axis. The tilt angle is larger than θ_p so that the effect of the TB's has been reduced substantially.

different crystal quality or a residual effect of TB pinning; that is, at large angles the intersection regions of the TB's with the vortices may act as "point" rather than planar pinning sites and this may drive the resistivity to lower values. Measurements are in progress to distinguish the effect of TB's on the melting transition at both small and large angles to determine whether the nature of the transition changes at some finite angle.

IV. CONCLUSION

We have measured the resistive transition in a magnetic field for $\mathbf{H}\|c$ for several crystals with three different Lorentz-force directions relative to the TB's. We find that the downturn toward zero resistivity at the shoulder in the transition becomes progressively steeper as the angle between the Lorentz force and TB's increases. We interpret this result as an increase of the pinning barriers as the Lorentz force is rotated toward the twin plane normal. The shoulder in the resistive transition has been shown directly to coincide with the onset of TB pinning by angular-dependent magnetoresistance measurements. Comparison of the strong and weak TB-pinning configurations and detwinned crystals reveals that the TB's are the pinning center causing the downturn to zero resistivity in twinned crystals in magnetic fields precisely aligned with the c axis. The angular-dependent pinning curves taken at temperatures below the shoulder are characterized by a depinning angle above which the TB's no longer effectively pin as planar defects. A comparison of the three Lorentz-force geometries for $\mathbf{H}\|c$ yields the observation that the depinning angle increases monotonically as the Lorentz force is rotated toward the TB normal. This increase is a direct manifestation of the anisotropy of the TB-pinning barriers and is consistent with the conjecture that these barriers increase as the angle between the Lorentz force and the twin boundaries becomes larger. For flux motion parallel to the twin boundaries, our measurements suggest that the dynamics is similar to that in the presence of point defects with an enhanced defect density. However, a dynamical description of flux motion normal to the twin boundaries requires that the planar nature of the twin boundaries, or the effect of correlated disorder, be considered.

Twin-boundary pinning was investigated for both $\mathbf{H}\|c$ and $\mathbf{H}\|ab$ on the same crystal using a contact geometry in which the current was applied normal to the TB's. The maximum Lorentz-force configuration ($\mathbf{H}\perp J$) was obtained for both magnetic-field orientations $\mathbf{H}\|c\|$TB and $\mathbf{H}\|ab\|$TB, making comparison unambiguous. The depinning angle for rotations off the c axis was found to be larger than that for rotations in the ab plane for $\mathbf{H}<4$ T. We find the depinning angle for $\mathbf{H}\|ab\|$TB to be relatively insensitive to magnetic field, whereas the depinning angle for rotations off the c axis decrease linearly with increasing magnetic field and lower temperature.

Twin-boundary pinning for $\mathbf{H}\|c$ was investigated below the shoulder in the liquid state for which the I-V characteristics were found to be linear. For small tilts off the c axis, a second kink in the resistive transition develops, below which non-Ohmic behavior was observed. This second kink evolves into the kink which we have identified as the onset of the flux-lattice melting transition for angles above the depinning angle. However, at low angles pinning by twin boundaries seems to suppress the melting transition and may alter the nature of the transition altogether.

ACKNOWLEDGMENTS

We would like to thank Ron Galicia and Joseph Soukup for their expertise and assistance in developing the computer software used for data acquisition. This work was supported by the U.S. Department of Energy, Basic Energy Sciences, Materials Science, under Contract No. W-31-109-ENG-38 (S.F., W.K.K., J.D., and G.W.C.) and the National Science Foundation, Office of Science and Technology, under Contract No. STC91-20000 (U.W. and V.M.V.), Science and Technology Center for Superconductivity. S.F. acknowledges partial support from the Division of Educational Programs, Argonne National Laboratory. M.K.S. acknowledges support from the Science and Engineering Research Semester (SERS) program, Division of Educational Programs, Argonne National Laboratory.

*Also at the Department of Physics, Purdue University, West Lafayette, IN 47907.

[1]T. T. M. Palstra, B. Batlogg, R. B. van Dover, L. F. Schneemeyer, and J. V. Waszczak, Appl. Phys. Lett. **54**, 763 (1989); Phys. Rev. B **41**, 6621 (1990).

[2]J. N. Li, K. Kadowaki, M. J. V. Menken, A. A. Menovsky, and J. J. M. Franse, Physica C **161**, 313 (1989).

[3]T. K. Worthington, F. H. Holtzberg, and C. Z. Feild, Cryogenics **30**, 417 (1990).

[4]V. M. Vinokur, M. V. Feigel'man, V. B. Geshkenbein, and A. I. Larkin, Phys. Rev. Lett. **65**, 259 (1990).

[5]M. C. Marchetti and D. R. Nelson, Phys. Rev. B **41**, 1910

(1990).
[6]M. C. Marchetti and D. R. Nelson, Phys. Rev. B **42**, 9938 (1990).
[7]R. H. Koch, V. Foglietti, W. J. Gallagher, G. Koren, A. Gupta, and M. P. A. Fisher, Phys. Rev. Lett. **63**, 1511 (1989).
[8]P. L. Gammel, L. F. Schneemeyer, and D. J. Bishop, Phys. Rev. Lett. **66**, 953 (1991).
[9]M. P. A. Fisher, Phys. Rev. Lett. **62**, 1415 (1989).
[10]H. Safar, P. L. Gammel, D. A. Huse, and D. J. Bishop, Phys. Rev. Lett. **69**, 824 (1992).
[11]T. K. Worthington, M. P. A. Fisher, D. A. Huse, John Toner, A. D. Marwick, T. Zabel, C. A. Field, and F. Holtzberg, Phys. Rev. B **46**, 11 854 (1992).
[12]W. K. Kwok, S. Fleshler, U. Welp, V. M. Vinokur, J. Downney, G. W. Crabtree, and M. M. Miller, Phys. Rev. Lett. **69**, 3370 (1992).
[13]U. Welp, M. Grimsditch, H. You, W. K. Kwok, M. M. Fang, G. W. Crabtree, and J. Z. Liu, Physica C **161**, 1 (1989).
[14]B. M. Vlcek, M. C. Frischherz, S. Fleshler, U. Welp, J. Z. Liu, K. G. Vandervoort, G. W. Crabtree, M. A. Kirk, J. Downey, J. Giapintzakis, and J. J. Farmer, Phys. Rev. B **46**, 6441 (1992).
[15]W. K. Kwok, U. Welp, G. W. Crabtree, K. G. Vandervoort, R. Hulscher, and J. Z. Liu, Phys. Rev. Lett. **64**, 966 (1990).
[16]J. N. Li, Z. Tarnawski, and J. J. M. Franse, Physica C **180**, 411 (1990).
[17]C. A. Durán, P. L. Gammel, R. Wolfe, V. J. Fratello, D. J. Bishop, J. P. Rice, and D. M. Ginsberg, Nature **357**, 474 (1992).
[18]U. Welp, W. K. Kwok, G. W. Crabtree, K. G. Vandervoort, and J. Z. Liu, Appl. Phys. Lett. **57**, 74 (1990).
[19]D. L. Kaiser, F. W. Gayle, L. J. Swartzendruber, L. H. Bennett, and R. D. McMichael, J. Appl. Phys. **70**, 5739 (1990).
[20]B. Roas, L. Schultz, and G. Saemann-Ischenko, Phys. Rev. Lett. **64**, 479 (1990).
[21]W. K. Kwok, S. Fleshler, U. Welp, V. M. Vinokur, J. Downey, and G. W. Crabtree, in *Advances in Superconductivity IV,* Proceedings of the 4th International Symposium on Superconductivity, edited by H. Hayakaswa and N. Koshizuka (Springer-Verlag, Tokyo, 1992), pp. 317–322.
[22]L. J. Swartzendruber, A. Roitburd, D. L. Kaiser, F. W. Gayle, and L. H. Bennett, Phys. Rev. Lett. **64**, 483 (1990).
[23]A. Umezawa, G. W. Crabtree, U. Welp, W. K. Kwok, K. G. Vandervoort, and J. Z. Liu, Phys. Rev. B **42**, 8744 (1990).
[24]J. Z. Liu, Y. X. Jia, R. N. Shelton, and M. J. Fluss, Phys. Rev. Lett. **66**, 1354 (1990).
[25]E. M. Gyorgy, R. B. van Dover, L. F. Schneemeyer, A. E. White, H. M. O'Bryan, R. J. Felder, J. V. Waszczak, and W. W. Rhodes, Appl. Phys. Lett. **56**, 2465 (1990).
[26]B. Jannosy, R. Hergt, and L. Fruchter, Physica C **170**, 22 (1990).
[27]R. Hergt, W. Andrä, and W. Schüppel, Phys. Status Solidi A **122**, K51 (1990); **123**, 255 (1991); R. Hergt, W. Andrä, R. Hiergeist, and J. Taubert, *ibid.* **129**, 1 (1992).
[28]G. J. Dolan, G. V. Chandrashekhar, T. R. Dinger, C. Feild, and F. Holtzberg, Phys. Rev. Lett. **62**, 827 (1989).
[29]L. Ya. Vinnikov, L. A. Gurevich, G. A. Yemelchenko, and Yu. A. Ossipyan, Solid State Commun. **67**, 421 (1988); L. Ya. Vinnikov, I. V. Grigor'eva, L. A. Gurevich, and A. E. Koshelev, Superconductivity **3**, 1121 (1990).
[30]I. V. Grigor'eva, L. A. Gurevich, and L. Ya. Vinnikov, Physica C **195**, 327 (1992).
[31]G. Blatter, J. Rhyner, and V. M. Vinokur, Phys. Rev. B **43**, 7826 (1991).
[32]D. L. Kaiser, F. Holtzberg, M. F. Chisholm, and T. K. Worthington, J. Cryst. Growth **85**, 593 (1987).
[33]W. K. Kwok, U. Welp, V. M. Vinokur, S. Fleshler, J. Downey, and G. W. Crabtree, Phys. Rev. Lett. **67**, 390 (1991).
[34]S. Fleshler, W. K. Kwok, U. Welp, J. Downey, and G. W. Crabtree, IEEE Trans. Magn. (to be published).
[35]G. W. Crabtree, W. K. Kwok, U. Welp, J. Downey, S. Fleshler, K. G. Vandervoort, and J. Z. Liu, Physica C **185-189**, 282 (1991).
[36]D. R. Nelson and H. S. Seung, Phys. Rev. B **39**, 9153 (1989).
[37]A. Sudbø and E. H. Brandt, Phys. Rev. Lett. **66**, 1781 (1991); Phys. Rev. B **43**, 10 482 (1991).
[38]M. C. Marchetti and D. R. Nelson, Physica C **174**, 40 (1991).
[39]D. R. Nelson and V. M. Vinokur, Phys. Rev. Lett. **68**, 2398 (1992).
[40]T. K. Worthington, W. J. Gallagher, D. L. Kaiser, F. H. Holtzberg, and T. R. Dinger, Physica C **153-155**, 32 (1988).